Article

SOURCE DATA | TRANSPARENT PROCESS

EMBO reports

Activation of hypothalamic RIP-Cre neurons promotes beiging of WAT via sympathetic nervous system

Baile Wang[1,2], Ang Li[3], Xiaomu Li[4], Philip WL Ho[2], Donghai Wu[5], Xiaoqi Wang[6], Zhuohao Liu[1,2], Kelvin KL Wu[7], Sonata SY Yau[8], Aimin Xu[1,2,9,*] & Kenneth KY Cheng[7,**]

Abstract

Activation of brown adipose tissue (BAT) and beige fat by cold increases energy expenditure. Although their activation is known to be differentially regulated in part by hypothalamus, the underlying neural pathways and populations remain poorly characterized. Here, we show that activation of rat-insulin-promoter-Cre (RIP-Cre) neurons in ventromedial hypothalamus (VMH) preferentially promotes recruitment of beige fat via a selective control of sympathetic nervous system (SNS) outflow to subcutaneous white adipose tissue (sWAT), but has no effect on BAT. Genetic ablation of APPL2 in RIP-Cre neurons diminishes beiging in sWAT without affecting BAT, leading to cold intolerance and obesity in mice. Such defects are reversed by activation of RIP-Cre neurons, inactivation of VMH AMPK, or treatment with a β3-adrenergic receptor agonist. Hypothalamic APPL2 enhances neuronal activation in VMH RIP-Cre neurons and raphe pallidus, thereby eliciting SNS outflow to sWAT and subsequent beiging. These data suggest that beige fat can be selectively activated by VMH RIP-Cre neurons, in which the APPL2–AMPK signaling axis is crucial for this defending mechanism to cold and obesity.

Keywords AMPK; beiging; hypothalamus; obesity; sympathetic nervous system

Subject Categories Metabolism; Neuroscience

DOI 10.15252/embr.201744977 | Received 8 August 2017 | Revised 23 January 2018 | Accepted 25 January 2018 | Published online 21 February 2018

EMBO Reports (2018) 19: e44977

See also: **M C Miletta & T L Horvath** (April 2018)

Introduction

Brown adipocytes dissipate nutritional energy into heat (known as adaptive thermogenesis) by uncoupling electron transport from ATP synthesis via the actions of uncoupling protein 1 (UCP1) in the mitochondria. It was initially believed that constitutive brown adipocytes could only be found in human infants or small rodents, but recent studies identified UCP1-positive brown adipocytes in subcutaneous white adipose tissue (sWAT), which are so-called "beige adipocytes", of human adults [1]. Although the origins of constitutive brown adipocytes and beige adipocytes are different, they both exhibit thermogenic capacity and protective effects on metabolic health [2]. The activity of beige cells is negatively associated with body mass index, adiposity, and age in humans [3,4]. Activation of classical brown adipose tissue (BAT) and/or beige adipocytes not only combats obesity via induction of energy expenditure, but also mitigates diabetes, dyslipidemia, and atherosclerosis via paracrine and/or endocrine manners in rodent models [5–10].

Thermogenesis and lipolysis in BAT and WAT are differentially regulated by the hypothalamus and elsewhere in the brain [11]. Different adipose tissues receive distinct sympathetic signals originating in the hypothalamus in response to nutritional and environmental challenges to maintain proper energy balance [12,13]. Upon cold exposure, beige adipocytes and classical brown adipocytes are activated and recruited by norepinephrine (NE) primarily released from sympathetic postganglionic neurons [1,14]. NE not only triggers lipolysis to generate free fatty acids (FFA) for activation of UCP1, but also induces UCP1 expression via a β3-adrenergic receptor-protein kinase A-cAMP-dependent pathway

1 State Key Laboratory of Pharmaceutical Biotechnology, The University of Hong Kong, Hong Kong, China
2 Department of Medicine, The University of Hong Kong, Hong Kong, China
3 Guangdong-Hong Kong-Macau Institute of CNS Regeneration, Joint International Research Laboratory of CNS Regeneration Ministry of Education, Guangdong Medical Key Laboratory of Brain Function and Diseases, Jinan University, Guangzhou, China
4 Department of Endocrinology and Metabolism, Zhongshan Hospital, Fudan University, Shanghai, China
5 Key Laboratory of Regenerative Biology and Guangdong Provincial, Key Laboratory of Stem Cell and Regenerative Medicine, Guangzhou Institute of Biomedicine and Health, Chinese Academy of Sciences, Guangzhou, China
6 Department of Surgery, The University of Hong Kong, Hong Kong, China
7 Department of Health Technology and Informatics, The Hong Kong Polytechnic University, Hong Kong, China
8 Department of Rehabilitation Science, The Hong Kong Polytechnic University, Hong Kong, China
9 Department of Pharmacology & Pharmacy, The University of Hong Kong, Hong Kong, China
*Corresponding author. Tel: +852 3917 9754; E-mail: amxu@hku.hk
**Corresponding author. Tel: +852 3400 8912; E-mail: kenneth.ky.cheng@polyu.edu.hk

[15]. Recent studies indicate that distinct hypothalamic neuronal populations [such as agouti-related protein (AgRP) neuron, proopiomelanocortin (POMC) neuron, and steroidogenic factor 1 (SF1) neuron] regulate brown and beige adipocyte thermogenesis, mainly via activation of sympathetic nervous system (SNS) [16–18]. Although both BAT and sWAT are innervated and controlled by SNS, dual PRV tract tracing experiment revealed that only ~10–20% of SNS circuitry to BAT and sWAT in hypothalamus is shared [13]. Furthermore, activation of AgRP neurons selectively suppresses beiging in WAT but has no obvious effect on BAT thermogenesis under fasting condition [16]. Despite these interesting findings, the role of hypothalamus in differential regulation of beiging and thermogenic programs in BAT and WAT under different nutritional and environmental cues are largely unknown.

APPL2, an adaptor protein containing pleckstrin homology (PH) domain, phosphotyrosine binding (PTB) domain, and leucine zipper motif, is a scaffold protein that transmits signals from early endosome to the nucleus by interacting with its close homolog APPL1 and/or the small GTPase Rab5 in response to extracellular stimuli [19,20]. We and others reported that this pair of adaptor proteins acts as a "Yin and Yang" regulator of adiponectin and insulin signaling [21,22]. APPL2 negatively controls insulin- or adiponectin-stimulated glucose uptake in skeletal muscle [21,22], whereas APPL1 exerts opposite actions [22,23]. In pancreatic β-cells, APPL1 facilitates glucose-stimulated insulin secretion by upregulating the expression of exocytotic machinery proteins via an Akt-dependent pathway and protects against β-cell apoptosis by inhibiting NF-κB activation [24,25]. Indeed, human subjects carrying loss-of-function mutation of APPL1 are diabetes and expression of APPL1 in human islets is positively correlated with glucose-stimulated insulin secretion [26].

To explore whether APPL2, like APPL1, plays a role in β-cell functions, we crossed APPL2$^{floxed/floxed}$ mice [21] with the transgenic mice expressing Cre recombinase under the control of rat insulin promoter (RIP). The crossed mice are so-called RIP-APPL2-KO mice. During the phenotypic characterization of RIP-APPL2-KO mice, we observed a marked increase in adiposity and impairment of adaptive thermogenesis. Given that Cre expression driven by RIP is not only expressed in pancreatic β-cells but also in the hypothalamus [27], we here explored the potential role of RIP-Cre neurons in adaptive thermogenesis and beiging of WAT, and investigated how they controlled energy homeostasis via SNS.

Results

Reduced energy expenditure and increased adiposity in RIP-APPL2-KO mice

As mentioned, Cre expression driven by RIP was observed in both pancreatic β-cells and different regions of hypothalamus [27]. We first examined expression of APPL2 in β-cells and the hypothalamus, and determined whether its expression is reduced in RIP-APPL2-KO mice. Immunohistochemical (IHC) staining revealed that APPL2 was abundantly expressed in the ventromedial hypothalamus (VMH), but was barely detectable in the arcuate nucleus (ARC) and paraventricular nucleus (PVN) of the hypothalamus (Fig EV1A). Next, we determined whether RIP-Cre neurons co-express with APPL2 and the VMH neuronal marker Nkx2.1 [28,29]. To this end, we generated a mouse model in which RIP-Cre neurons were labeled with green fluorescent protein (GFP) by crossing RIP-Cre mice with Z/EG mice (a double-reporter mouse line that expresses enhanced GFP upon Cre-mediated excision [30]). This model is so-called "RIP-Cre-GFP" mouse. Immunofluorescence staining showed that ~70 and ~15% RIP-Cre neurons in the VMH expressed APPL2 and Nkx2.1, respectively, in this mouse model (Fig EV1B and C). In addition, APPL2, like APPL1 [24], was expressed in pancreatic β-cells (Fig EV2A). Protein expression of APPL2 was markedly reduced in VMH and pancreatic β-cells but not in the liver of RIP-APPL2-KO mice when compared to their wild-type (WT) littermates (Fig EV2A–C). Expression of APPL1 in the hypothalamus was comparable between RIP-APPL2-KO mice and their WT controls (Fig EV2D). RIP-Cre-mediated deletion of APPL2 had no obvious effect on circulating level of insulin under fed condition (Appendix Fig S1A). RIP-APPL2-KO mice displayed significant higher fat content when fed with a standard chow (STC) or a high-fat diet (HFD) compared to their WT littermates or RIP-Cre controls, whereas body weight was similar among the three genotypes (Fig 1A and B). On the other hand, RIP-APPL2-KO mice had lower lean mass than WT controls under HFD but not STC feeding (Appendix Fig S1B). Body length was similar between RIP-APPL2-KO mice and their WT littermates (Appendix Fig S1C), suggesting that RIP-Cre-mediated deletion of APPL2 has no effect on growth. Since RIP-Cre control mice and WT littermates displayed similar adiposity, only WT littermates were included in all subsequent experiments. Weights of sWAT and eWAT but not interscapular BAT were increased in 22-week-old RIP-APPL2-KO mice fed with STC or HFD (Fig 1C). Hematoxylin and eosin (H&E) staining revealed that the size of adipocyte was slightly increased in sWAT and eWAT but not in BAT of RIP-APPL2-KO mice (Fig 1D–F). The increased adiposity was due to reduced energy expenditure (Fig 1G and H), while food intake, respiratory exchange ratio (RER), and locomotor activity remained unchanged in RIP-APPL2-KO mice fed with STC or HFD (Appendix Fig S1D–F).

Defective cold- and diet-induced adaptive thermogenesis in RIP-APPL2-KO mice

To investigate the underlying cause of reduced energy expenditure in RIP-APPL2-KO mice, we assessed adaptive thermogenesis in response to different environmental and nutritional challenges including short-term cold exposure, starvation, and short-term ingestion of HFD [31]. Energy expenditure was dramatically induced in WT controls when the diet was switched from STC to HFD; however, such an induction was modestly diminished in RIP-APPL2-KO mice (Fig 1G and H). Of note, lean mass and food consumption during the diet switch was similar among the two genotypes (Appendix Fig S1G and H). Furthermore, RIP-APPL2-KO mice were more cold-sensitive, which was accompanied by defective cold-induced lipolysis (Fig 2A–D). In contrast, the adaption to starvation, such as lipolysis and inhibition of adaptive thermogenesis, was comparable among RIP-APPL2-KO mice and their WT controls (Appendix Fig S2A–D).

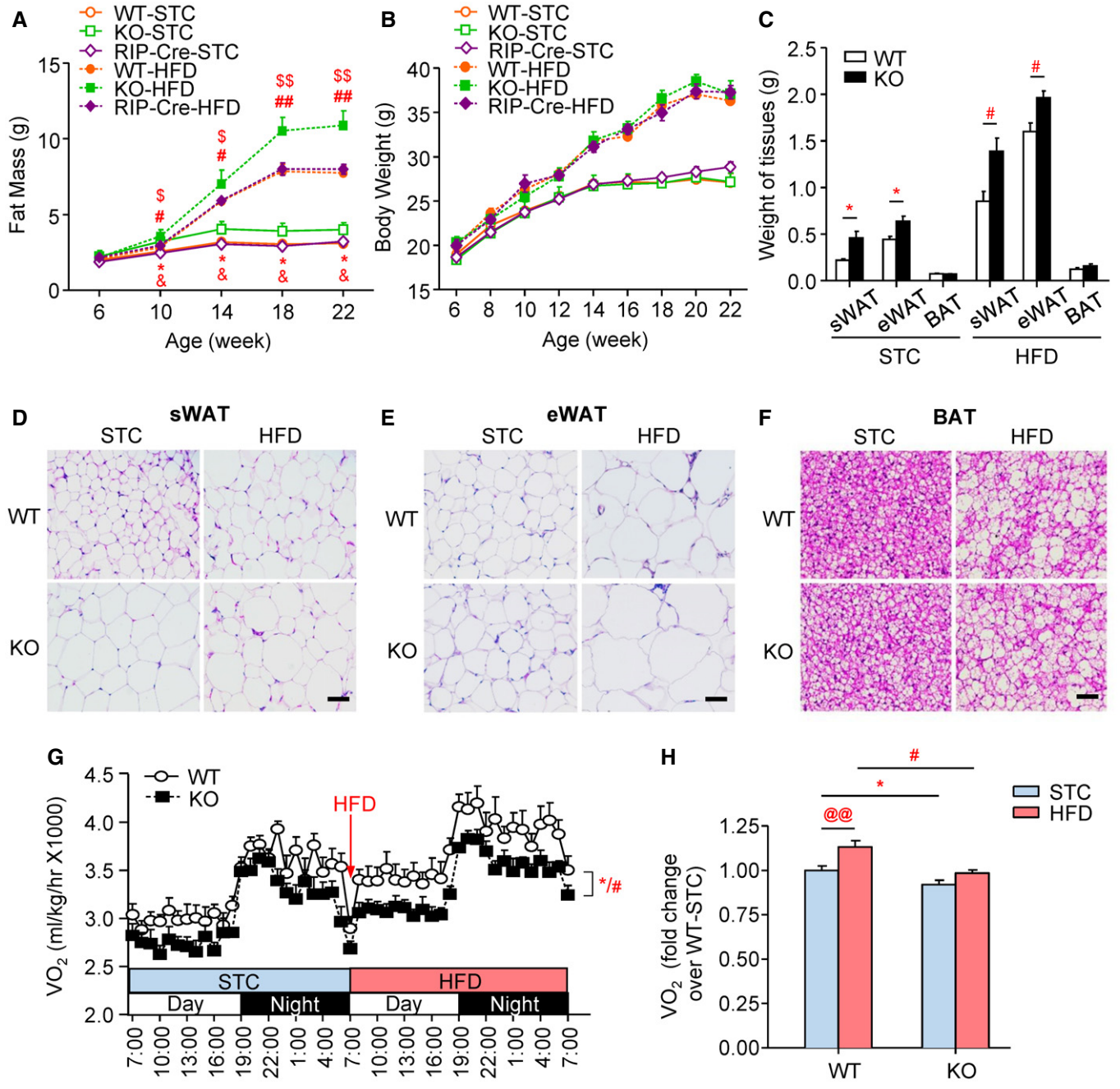

Figure 1. RIP-APPL2-KO mice display increased adiposity and reduced energy expenditure.

Six-week-old male RIP-APPL2-KO mice and their wild-type (WT) littermates and RIP-Cre control mice were fed with STC or HFD for indicated time points.

A Fat mass.

B Body weight.

C Weights of sWAT, eWAT, and interscapular BAT of the 22-week-old mice.

D–F Representative images of H&E staining of sWAT (D), eWAT (E), and BAT (F) of the 22-week-old mice.

G, H Measurement of oxygen consumption (VO_2) in the 14-week-old mice under STC feeding condition and a switch to HFD feeding as indicated by the arrow.

Data information: $n = 5$ for each group. Data are represented as mean ± SEM. $^{*}P < 0.05$ (WT-STC vs. KO-STC), $^{\#}P < 0.05$, $^{\#\#}P < 0.01$ (WT-HFD vs. KO-HFD), $^{@@}P < 0.01$ (WT-STC vs. WT-HFD), $^{\$}P < 0.05$, $^{\$\$}P < 0.01$ (KO-HFD vs. RIP-Cre-HFD), $^{\&}P < 0.05$ (KO-STC and RIP-Cre-STC); two-tailed independent Student's *t*-test. Scale bar: 50 μm.

As lipolysis in WAT is indispensable for supplying free fatty acids for BAT thermogenesis during cold challenge [32,33], we measured activity of hormone-sensitive lipase (HSL; a major lipase responsible for catecholamine-induced lipolysis in adipocytes under cold environment). Immunoblotting analysis demonstrated that cold exposure dramatically induced phosphorylation of HSL at serine 660 in

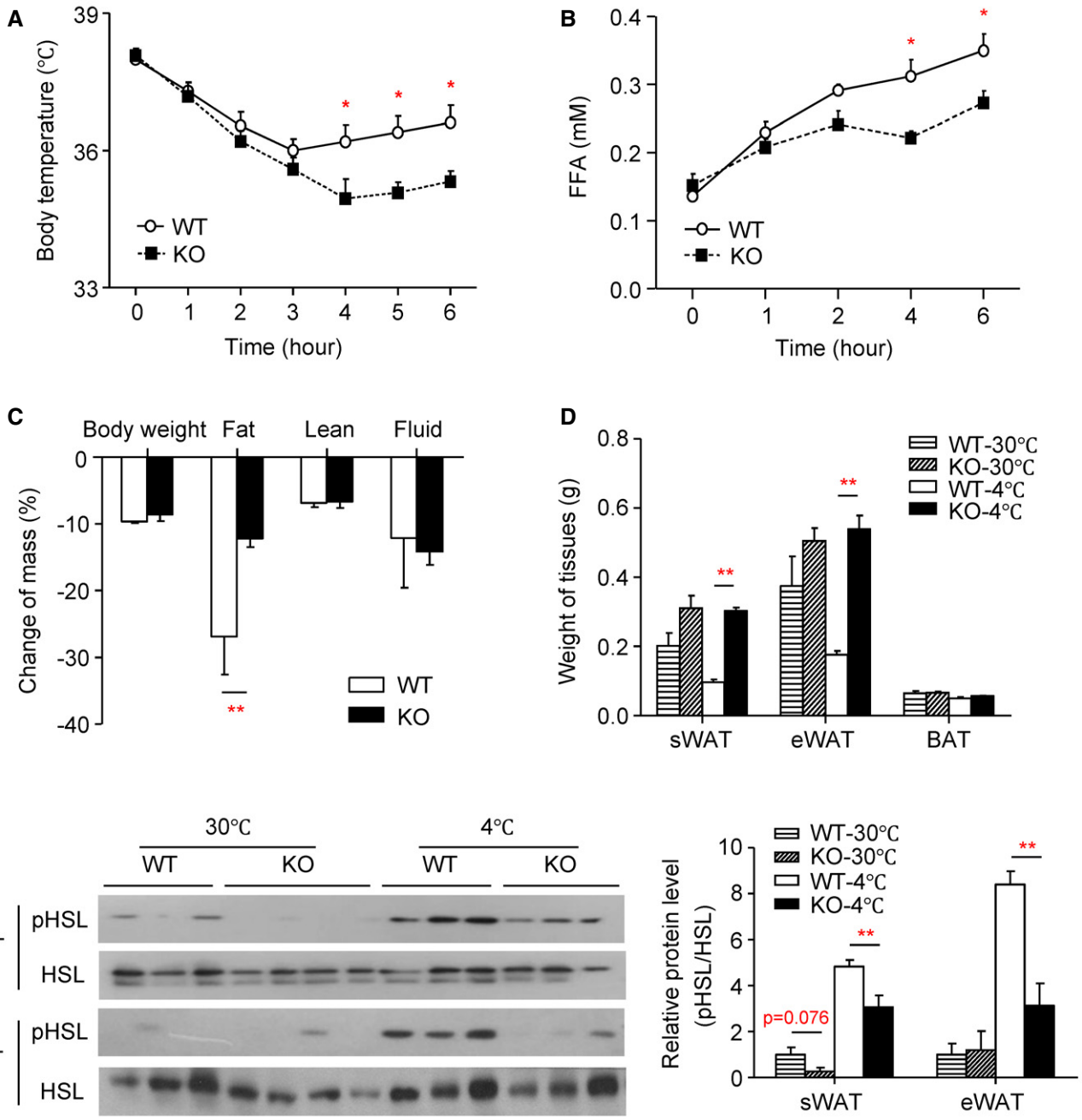

Figure 2. RIP-APPL2-KO mice exhibit impaired cold-induced thermogenesis and lipolysis.

A–C Twelve-week-old male RIP-APPL2-KO mice and their WT littermates were maintained at thermoneutral condition (30°C) for 2 weeks, followed by acute cold exposure (4°C) for 6 h as indicated. (A) Core body temperature and (B) serum level of FFA during cold exposure. (C) Change in body weight and body composition upon cold challenge. Data are expressed as percentage of change in mass relative to the thermoneutral condition.

D, E Adipose tissues were isolated from the mice kept at thermonetural environment for 2 weeks with or without cold exposure for 6 h. (D) Weights of sWAT, eWAT, and BAT. (E) The isolated adipose tissues were subjected to immunoblotting using an antibody against phospho-HSL (serine 660) or HSL as indicated. Representative immunoblotting images are shown. The right panel is the densitometric analysis for the relative abundance of phospho-HSL normalized with HSL.

Data information: $n = 5$. Data are represented as mean ± SEM. $^*P < 0.05$, $^{**}P < 0.01$ (two-tailed independent Student's *t*-test).
Source data are available online for this figure.

sWAT and eWAT of WT controls, and such an induction was largely attenuated in RIP-APPL2-KO mice (Fig 2E). Collectively, these data suggest that APPL2 is essential for cold- and diet-induced adaptive thermogenesis but not starvation response.

Beiging of sWAT is disrupted in RIP-APPL2-KO mice

To test whether RIP-mediated deletion of APPL2 impairs cold-induced activation of BAT and beiging in sWAT, we subjected RIP-

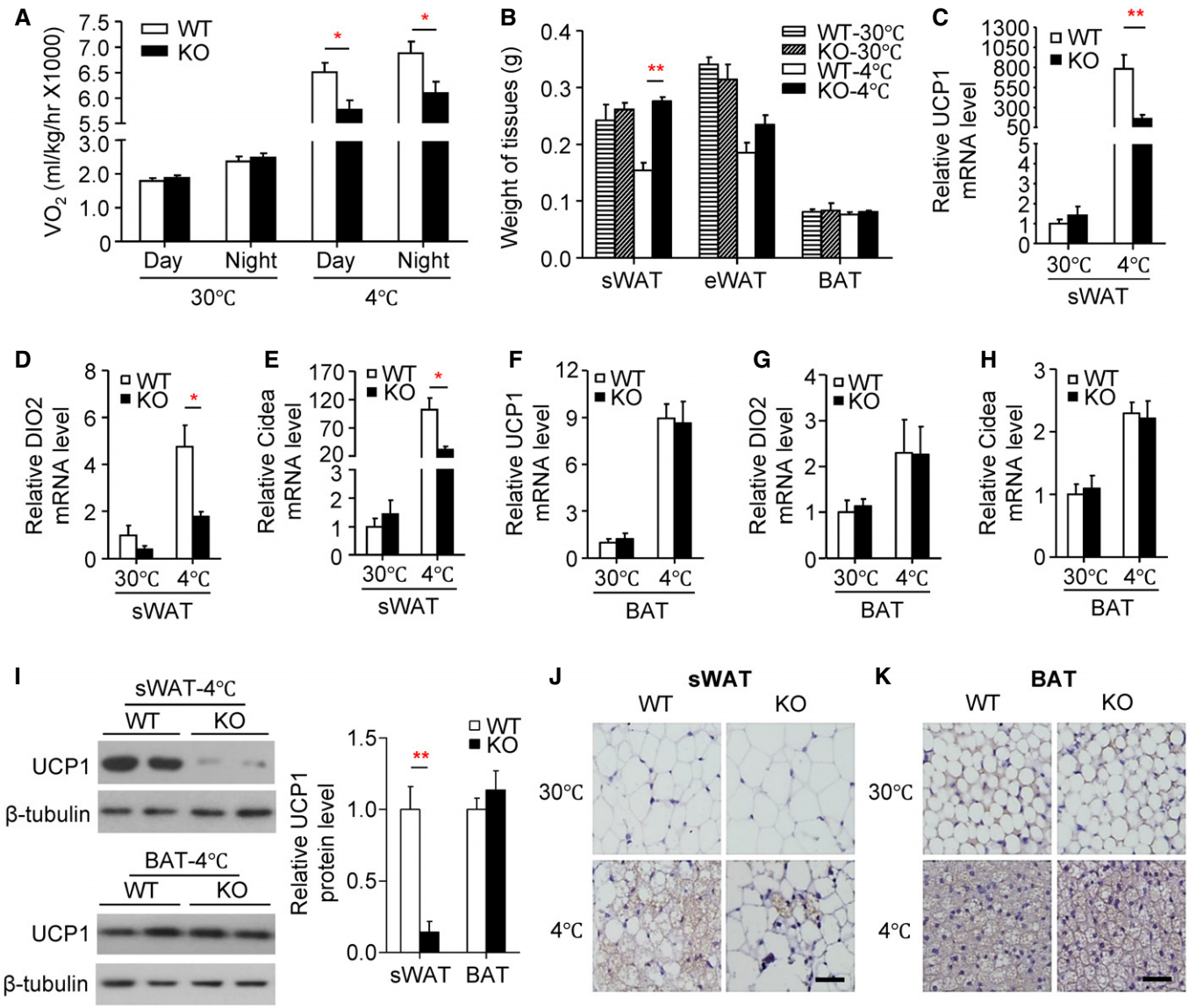

Figure 3. RIP-mediated deletion of APPL2 impairs cold-induced beiging in sWAT.

Twelve-week-old male RIP-APPL2-KO mice and their WT littermates were kept at thermoneutral condition (30°C) for 2 weeks or at cold room (4°C) for 10 days. Fat depots were collected for further analysis.

A Oxygen consumption.

B Weights of sWAT, eWAT, and BAT.

C–H The mRNA levels of UCP1, DIO2, and Cidea in sWAT (C–E) and BAT (F–H) were quantified by real-time quantitative PCR and normalized against 18S.

I Immunoblotting analysis of UCP1 and β-tubulin in sWAT (upper panel) and BAT (lower panel). The right panel represents the fold change of UCP1 relative to β-tubulin levels as determined by the densitometric analysis.

J, K Representative images of immunohistochemical (IHC) staining with an anti-UCP1 antibody in sWAT (J) and BAT (K) of the mice.

Data information: $n = 5$ for each group. Data are represented as fold change over WT-30°C and mean ± SEM. $^*P < 0.05$, $^{**}P < 0.01$ (two-tailed independent Student's *t*-test). Scale bar: 50 μm.

Source data are available online for this figure.

APPL2-KO mice and WT controls to cold environment for 10 days. Cold acclimation upregulated whole-body energy expenditure and reduced the mass of sWAT and eWAT in WT controls, whereas RIP-mediated deletion of APPL2 diminished these cold effects (Fig 3A and B). Cold-induced upregulation of thermogenic and beiging genes, including *UCP1*, type II iodothyronine deiodinase (*Dio2*), and cell death-inducing DFFA-like effector a (*Cidea*), was partially abolished in sWAT, but not in BAT, of RIP-APPL2-KO mice when compared to their WT controls (Fig 3C–H). Immunoblotting and immunohistological analyses confirmed that protein expression of UCP1 was reduced in sWAT but not in BAT of RIP-APPL2-KO mice after cold acclimation (Fig 3I–K).

SNS-dependent beiging in sWAT is impaired in RIP-APPL2-KO mice

Cold can induce beiging of WAT by activating hypothalamic neurons via regulating SNS tone [16,17]. Next, we tested whether the defective beiging in RIP-APPL2-KO mice is due to impairment of hypothalamus–SNS axis. Expression of tyrosine hydroxylase (the rate-limiting enzyme in norepinephrine biosynthesis and as a marker of sympathetic neurons and their activity) and norepinephrine content in sWAT but not in BAT, eWAT, liver, and kidney of RIP-APPL2-KO mice were significantly decreased compared to WT littermates after cold acclimation for 10 days, indicating that sympathetic outflow to sWAT was selectively diminished (Fig 4A–C). Treatment with the β3-adrenergic receptor agonist CL-316243 reversed the impaired beiging program in sWAT of RIP-APPL2-KO mice (Fig EV3A–C), suggesting that the defect does not lie in sWAT but presumably in the hypothalamus.

Raphe pallidus (RPa) in brain stem receives signals from the hypothalamic nuclei and transmits through sympathetic nerves to adipose tissues, leading to BAT thermogenesis and WAT beiging [13,34]. We next measured neuronal activity in RPa by immunohistochemical staining for c-Fos (as a surrogate for neuronal activity). Ten-day cold exposure dramatically increased c-Fos immunoreactivity in the RPa of WT controls, but this phenomenon was partially abolished in RIP-APPL2-KO mice (Fig 4D and E). Taken together, these findings indicate that the defective beiging of WAT in RIP-APPL2-KO mice is due to reduced sympathetic activity.

AAV-mediated deletion of APPL2 in VMH RIP-Cre neurons recapitulates the null phenotypes of RIP-APPL2-KO mice

The defects in RIP-APPL2-KO mice might be due to deletion of APPL2 in β-cells and/or RIP-Cre neurons. We next specifically deleted APPL2 in RIP-Cre neurons by stereotaxically injecting adeno-associated virus (AAV) encoding Cre recombinase under the control of RIP promoter into the VMH of 6-week-old male APPL2floxed/floxed mice (so-called VMH-RIP-APPL2-KO mice). We firstly confirmed the accurate injection and specific expression of AAV-RIP-GFP in the VMH (Appendix Fig S3A and B). Efficiency of APPL2 deletion in RIP-Cre neurons was verified by examining the expression levels of Cre and APPL2 using IHC staining (Fig 5A). This analysis revealed that APPL2 was decreased in neurons expressing Cre recombinase when compared to those expressing GFP (Fig 5A). Deletion of APPL2 in VMH RIP-Cre neurons had no obvious effect on body weight, food intake, RER, and locomotor activity (Appendix Fig S4A–D), but gradually increased adiposity and diminished energy expenditure (Fig 5B and C). Like RIP-APPL2-KO mice, VMH-RIP-APPL2-KO mice exhibited cold intolerance and impairment of cold-induced thermogenesis, beiging program, and SNS outflow in sWAT, when compared to the GFP controls (Fig 5D–I), whereas UCP1 expression and SNS activity in BAT were comparable between the two groups (Fig 5F–I). Notably, the defect in sWAT beiging was also associated with reduced c-Fos immunoreactivity in RPa (Fig 5J).

Activation of VMH RIP-Cre neurons rescues the impairment of sWAT beiging in RIP-APPL2-KO mice

Immunohistochemical staining revealed that deletion of APPL2 led to reduced neuronal activity in RIP neurons, as evidenced by reduced c-Fos-positive RIP-Cre neurons in the VMH of RIP-APPL2-KO mice after cold exposure for 10 days (Fig EV4A–C). To test whether activation of RIP-Cre neurons in the VMH can reverse the defective beiging in RIP-APPL2-KO mice, we employed a pharmacogenetic approach known as designer receptors exclusively activated by designer drugs (DREADD). The stimulatory DREADD, hM3Dq, can depolarize and activate neurons upon stimulation with brain-penetrable ligand clozapine-N-oxide (CNO), a pharmacologically inert ligand without any effect on adaptive thermogenesis [35]. The Cre recombinase-dependent AAV with hM3Dq was bilaterally injected into VMH of RIP-APPL2-KO mice and their WT littermates (so-called $hM3D_{Gq}$KO and $hM3D_{Gq}$WT mice, respectively), followed by treatment with CNO to activate the RIP-Cre neurons or vehicle as control under cold environment (Fig 6A). Expression of mCherry fluorescent protein was only detected in the VMH of $hM3D_{Gq}$KO mice but not in $hM3D_{Gq}$WT controls (because they do not express Cre recombinase that mediates expression of hM3Dq; Fig 6B). Treatment with CNO dramatically increased c-Fos immunoreactivity in the VMH of $hM3D_{Gq}$KO mice when compared to those treated with vehicle control, confirming that RIP-Cre neurons in VMH are activated (Fig 6C). In addition, CNO treatment reversed the reduction in neuronal activity in VMH of RIP-APPL2-KO mice (Fig 6C). The cold intolerance, reduced oxygen consumption, aberrant thermogenic program, and diminished SNS activation of sWAT in $hM3D_{Gq}$KO mice were reversed by activation of RIP-Cre neurons when compared to $hM3D_{Gq}$KO mice treated with vehicle (Fig 6D–I). In contrast, activation of RIP-Cre neurons, again, had no effect on BAT metabolism, food intake, RER, and locomotor activity (Fig 6G–I and Appendix Fig S5).

APPL2 regulates sWAT beiging via the VMH AMPK–SNS axis

APPL2 is a scaffold protein tethering different signaling molecules, such as APPL1, Rab5, Akt, and AMPK, to exert its metabolic actions in peripheral tissues [19,21,22]. Since the hypothalamic AMP-activated protein kinase (AMPK) and Akt signaling axis have been shown to control adipose tissue thermogenesis and beiging [17,36,37], we tested whether activities of AMPK and Akt were altered by deletion of APPL2 in hypothalamus. Immunoblotting analysis showed that AMPK phosphorylation at threonine 172 and its downstream ACC phosphorylation at serine 79 but not Akt phosphorylation at serine 473 was elevated in hypothalamus of RIP-APPL2-KO mice under cold condition (Fig 7A and B). Next, we investigated whether inactivation of VMH AMPK was able to rescue the APPL2-null phenotypes. To this end, we injected AAV encoding dominant-negative form of AMPK (AAV-DN-AMPK) or GFP (AAV-GFP) into VMH of RIP-APPL2-KO mice and its WT littermates. Immunoblotting analysis revealed that phosphorylations of AMPK and its downstream ACC were reduced in hypothalamus of RIP-APPL2-KO mice injected with AAV-DN-AMPK when compared to those injected with AAV-GFP (Fig 7C). The oxygen consumption, cold tolerance, beiging program, TH expression in sWAT, and neuronal activity in RPa were restored by AMPK

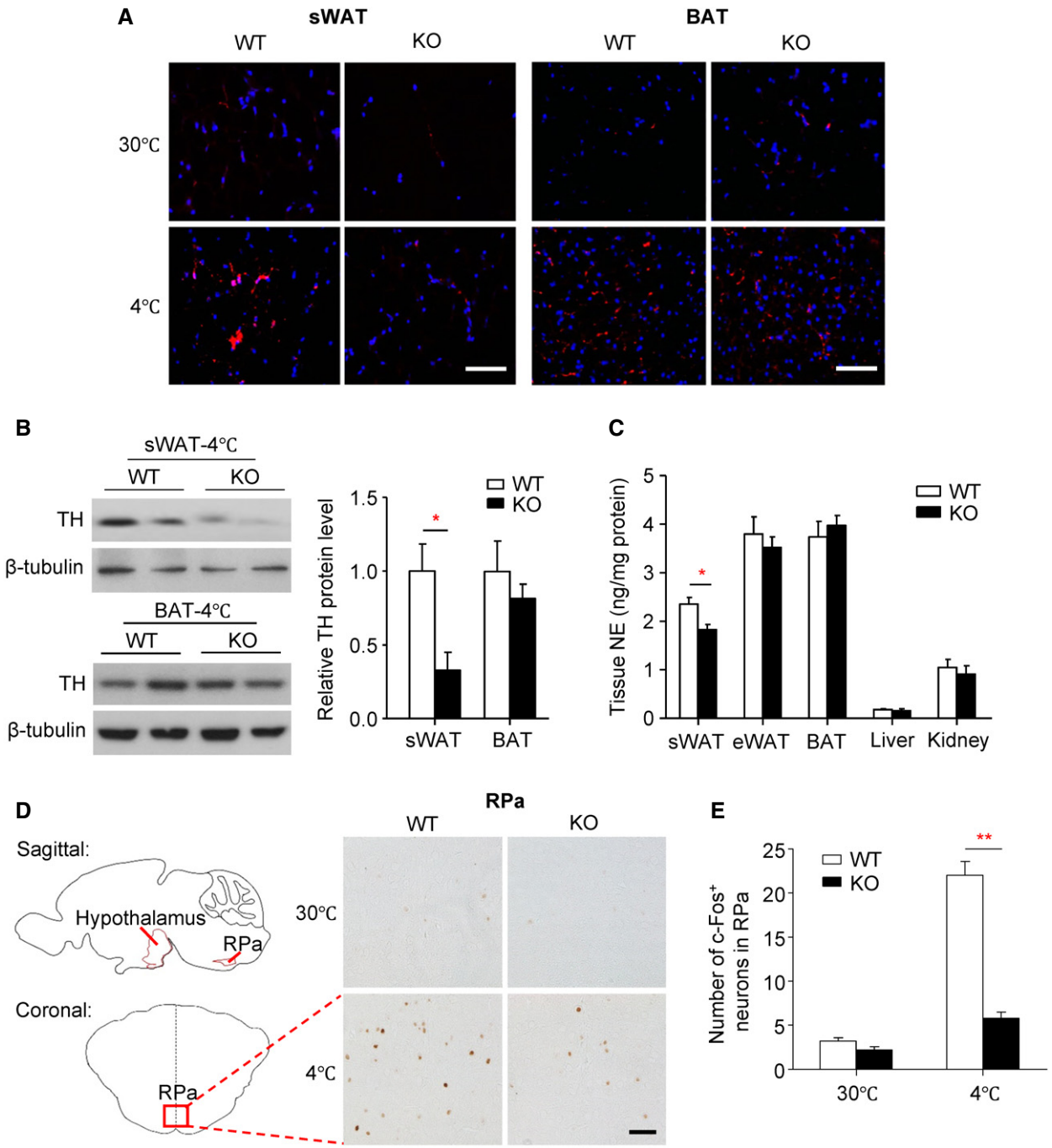

Figure 4. Cold-induced activation of sympathetic outflow to sWAT is impaired in RIP-APPL2-KO mice.

Twelve-week-old male RIP-APPL2-KO mice and their WT littermates fed with STC were housed under thermoneutral condition (30°C) for 2 weeks or under cold exposure (4°C) for 10 days.

A Representative images of IHC staining with an antibody against tyrosine hydroxylase (TH, red) in sWAT and BAT of the above mice. The nuclei were stained with DAPI (blue).

B Immunoblotting analysis of TH expression in sWAT (upper panel) and BAT (lower panel). The right panel represents densitometric analysis for the relative abundance of TH normalized with β-tubulin.

C NE contents (normalized with total protein concentration) in sWAT, eWAT, BAT, liver, and kidney of the mice after 10-day cold exposure.

D Representative images of IHC staining with an antibody against c-Fos in raphe pallidus (RPa) of the mice. The left panel is diagram illustrating the location of RPa.

E Quantification of the number of c-Fos-positive neurons in the RPa.

Data information: $n = 5$ for each group. Data are represented as mean ± SEM. $^*P < 0.05$, $^{**}P < 0.01$ (two-tailed independent Student's t-test). Scale bar: 50 μm.
Source data are available online for this figure.

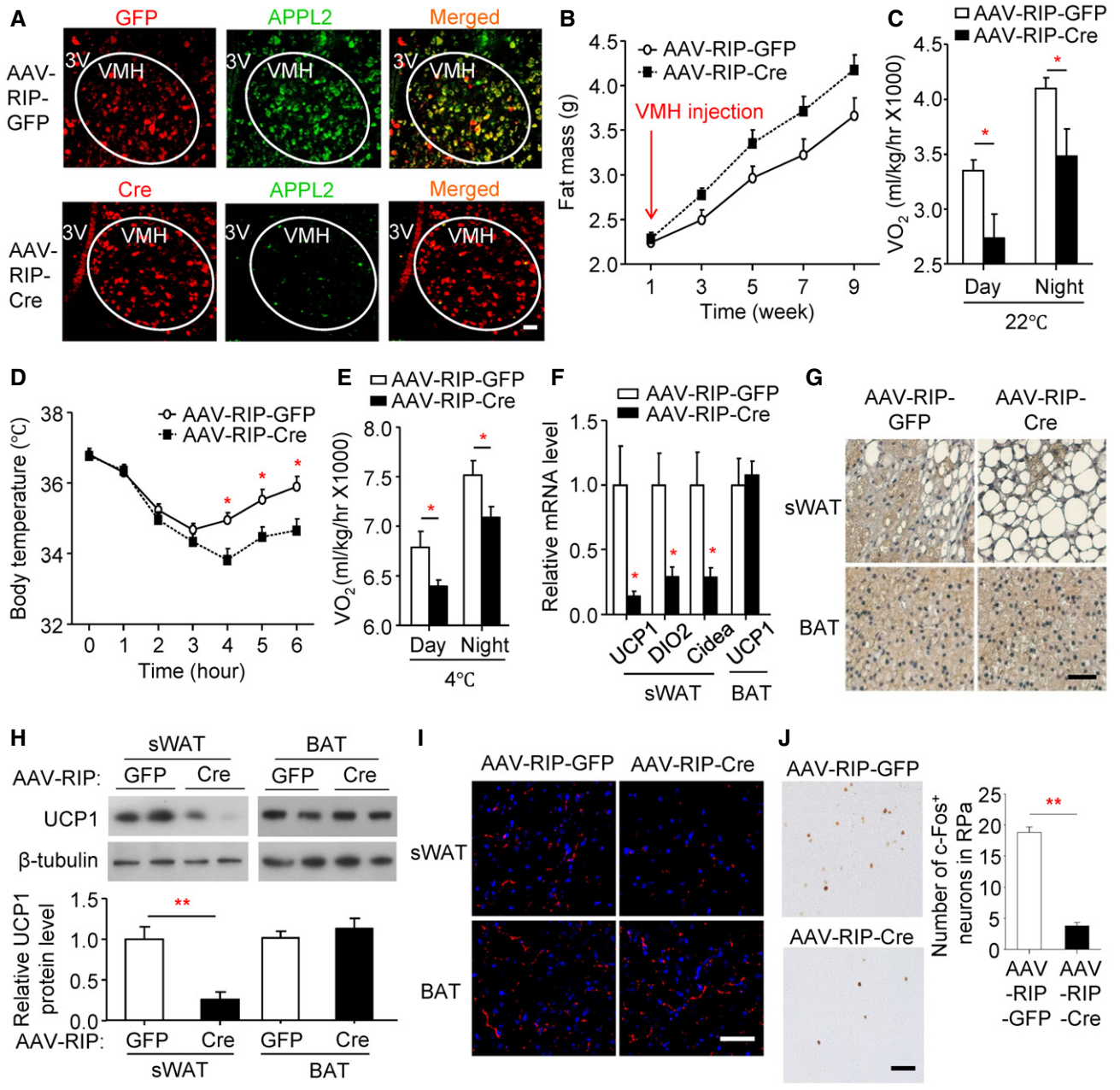

Figure 5. Adeno-associated virus (AAV)-mediated deletion of APPL2 in VMH RIP-Cre neurons selectively impedes cold-induced thermogenic program in sWAT.

Six-week-old male APPL2$^{floxed/floxed}$ mice were bilaterally injected with 2 × 10^9 viral particles of AAV-RIP-GFP or AAV-RIP-Cre into the hypothalamic VMH region, followed by 3-week post-surgery recovery.

A Representative images of IHC staining of GFP (upper panel, red, Santa Cruz #sc-8334), Cre (lower panel, red, Millipore #69050), and APPL2 (green, Abnova #H00055198-B01P) in VMH of mice after injection with indicated AAV for 3 weeks.

B Fat mass.

C Oxygen consumption under room temperature (22°C) at the 4th week after AAV injection.

D The mice were subjected to acute cold exposure (4°C) for 6 h at the 5th week after AAV injection. Core body temperature was measured.

E–J The mice were subjected to 10-day cold acclimation (4°C) at the 6th week after AAV injection. (E) Oxygen consumption after 8-day cold challenge. (F) mRNA levels of UCP1, DIO2, and Cidea normalized with 18S in sWAT and BAT of the mice. (G) Representative images of IHC staining of UCP1 in sections of sWAT and BAT. (H) Immunoblotting analysis of UCP1 in sWAT and BAT. The bar chart in the lower panel represents densitometric analysis for the relative abundance of UCP1 normalized with β-tubulin. (I) Representative images of IHC staining of TH (red) and DAPI (blue) in sections of sWAT and BAT of the mice after 10-day cold acclimation. (J) Representative images of IHC staining of c-Fos in RPa of the AAV-injected mice with 10-day cold acclimation. The right panel represents the quantification of the number of c-Fos-positive neurons in the RPa.

Data information: Data are represented as mean ± SEM. *P < 0.05, **P < 0.01 (two-tailed independent Student's t-test). (A–G) n = 6. (H–J) n = 5. Scale bars: (A) 100 μm, (G, I, J) 50 μm.
Source data are available online for this figure.

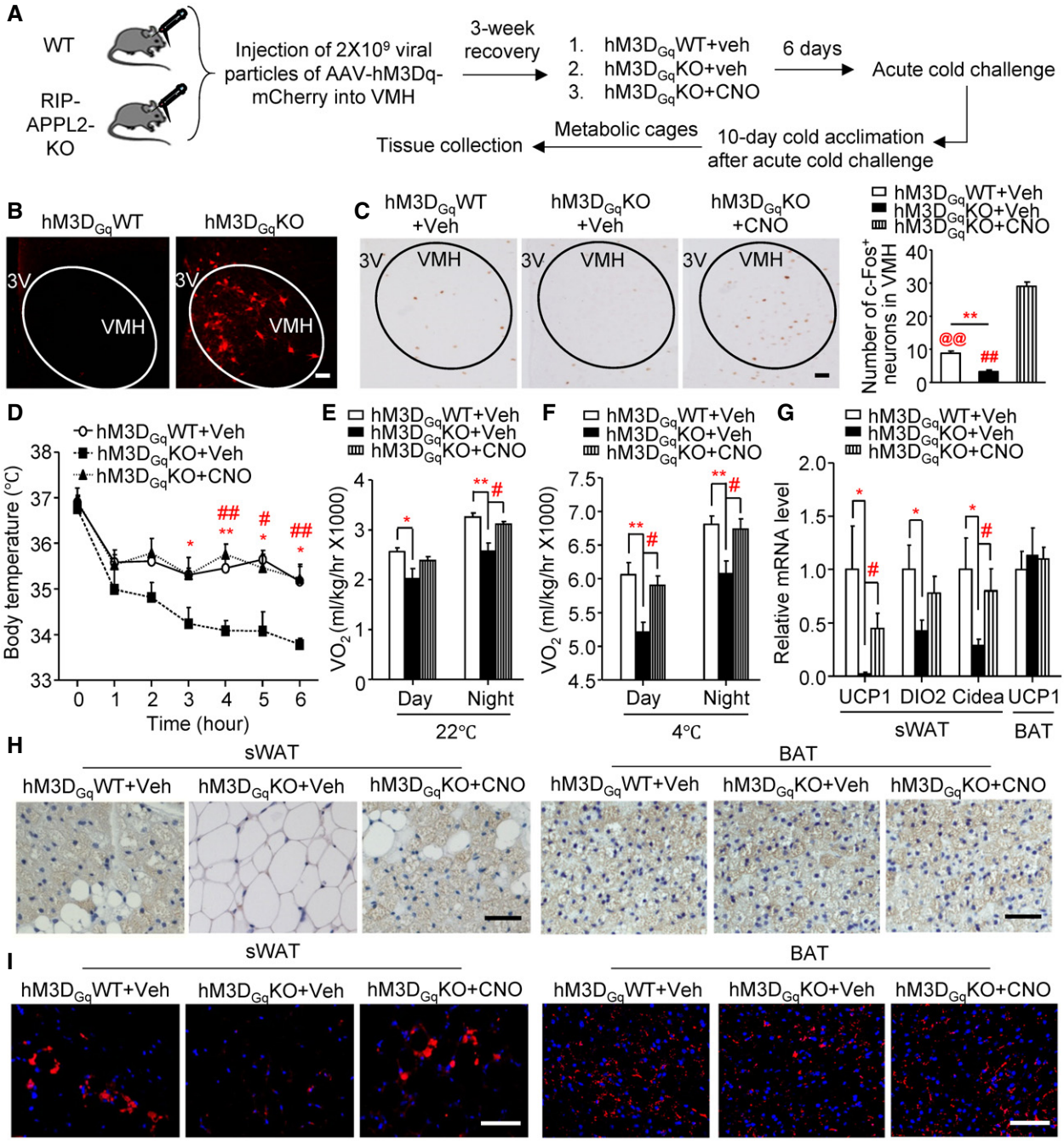

Figure 6. Activation of RIP-Cre neurons rescues the defective beiging in sWAT of RIP-APPL2-KO mice.

A Nine-week-old male RIP-APPL2-KO mice and their WT littermates were bilaterally injected with 2×10^9 viral particles of AAV-hM3Dq-mCherry into VMH to generate $hM3D_{Gq}$WT and $hM3D_{Gq}$KO mice, respectively. 3 weeks after injection, the mice were intraperitoneally injected with CNO (0.3 mg/kg) or saline (as vehicle) for 6 days at room temperature, followed by cold exposure for 10 days. CNO was continuously injected in a daily manner during cold exposure. The first day of CNO injection is defined as day 1.

B mCherry fluorescent signal (red) was directly examined under a fluorescent microscope. Representative images were shown.

C Representative images of IHC staining of c-Fos in VMH. The right panel represents the quantification of the number of c-Fos-positive neurons in the VMH.

D Core body temperature of mice during cold exposure at day 7.

E Oxygen consumption of mice under 22°C at day 4.

F Oxygen consumption under 4°C at day 14.

G mRNA levels of UCP1, DIO2, and Cidea normalized with 18S in sWAT and BAT (day 16).

H, I Representative images of IHC staining of UCP1 (H) and TH (red, panel I) of sWAT and BAT sections (day 16). (I) The nuclei were stained with DAPI (blue).

Data information: $n = 5$. Data are represented as mean ± SEM. $^*P < 0.05$, $^{**}P < 0.01$ ($hM3D_{Gq}$WT + Veh vs. $hM3D_{Gq}$KO + Veh), $^{\#}P < 0.05$, $^{\#\#}P < 0.01$, ($hM3D_{Gq}$KO + Veh vs. $hM3D_{Gq}$KO + CNO), $^{@@}P < 0.01$ ($hM3D_{Gq}$WT + Veh vs. $hM3D_{Gq}$KO + CNO); two-tailed independent Student's *t*-test. Scale bar: 50 μm.

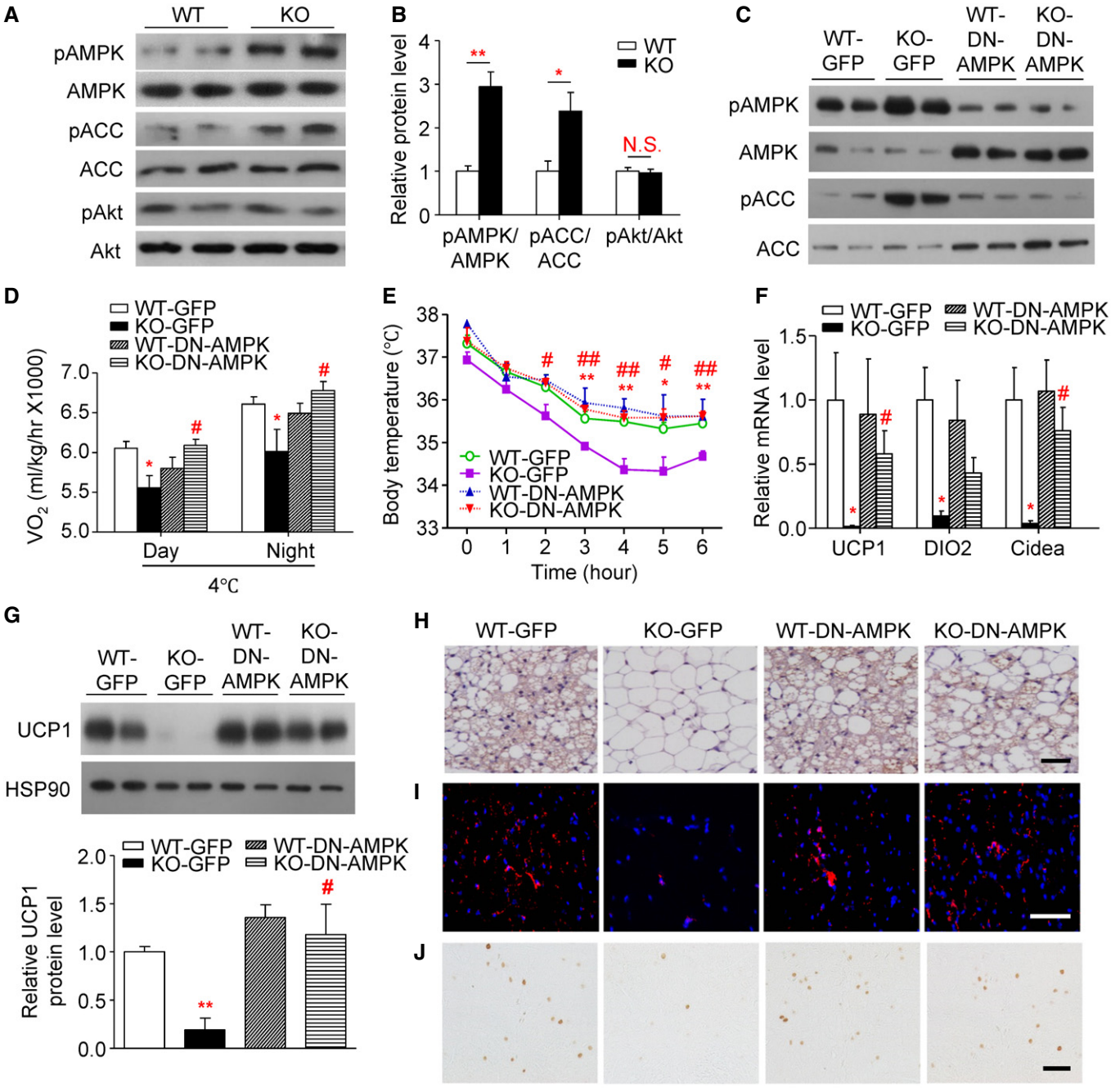

Figure 7. Inhibition of AMPKα activity in VMH restores beiging of sWAT in RIP-APPL2-KO mice.

A, B Twelve-week-old male RIP-APPL2-KO mice and their WT littermates fed with STC and housed at cold room (4°C) for 10 days were used. (A) Immunoblotting analysis of phospho-AMPK at threonine 172 (pAMPK), total AMPK, phospho-ACC at serine 79 (pACC), total ACC, phospho-Akt at serine 473 (pAkt), and total Akt in hypothalamus of the mice. (B) The bar chart is densitometric analysis of relative abundance of pAMPK, pACC, and pAkt normalized with total AMPK, ACC, and Akt, respectively.

C–J Twelve-week-old male RIP-APPL2-KO mice and their WT littermates were bilaterally injected with 2×10^9 viral particles of either AAV-GFP or AAV-DN-AMPK into VMH, followed by 3-week post-surgery recovery. The first week of AAV injection is defined as week-1. (C) Immunoblotting analysis of pAMPK, total AMPK, pACC, and total ACC in hypothalamus of the AAV-injected mice at week-8. (D) Oxygen consumption of the AAV-injected mice under 4°C at week-6. (E) Core body temperature upon acute cold exposure at week-5. (F) mRNA levels of UCP1, DIO2, and Cidea normalized with 18S in sWAT at week-8. (G) Immunoblotting analysis of UCP1 in sWAT at week-8. The lower panel is densitometric analysis of UCP1 expression relative to HSP90. (H, I) Representative images of IHC staining of UCP1 (H) and TH (red, panel I) of sWAT sections at week-8. (J) Representative images of IHC staining of c-Fos in RPa at week-8.

Data information: $n = 5$. Data are represented as mean ± SEM. $^*P < 0.05$, $^{**}P < 0.01$ (WT vs. KO or WT-GFP vs. KO-GFP), $^{\#}P < 0.05$, $^{\#\#}P < 0.01$ (KO-GFP vs. KO-DN-AMPK). N.S., not significant (two-tailed independent Student's *t*-test). Scale bar: 50 μm.
Source data are available online for this figure.

inactivation in RIP-APPL2-KO mice to a level similar to their WT controls (Fig 7D–J).

Activation of RIP-Cre neurons in VMH enhances beiging of sWAT and adaptive thermogenesis

A previous study demonstrated that activation of RIP-Cre neurons in ARC by pharmacogenetic method enhances BAT thermogenesis [38], whereas the precise role of RIP-Cre neurons in VMH in the regulation of beiging and sympathetic circuits of sWAT is still unknown. To investigate the effect of activation of RIP-Cre neurons in VMH on energy balance and adipose tissue functions, we injected Cre recombinase-dependent AAV with hM3Dq into VMH of RIP-Cre mice (so-called $hM3D_{Gq}$RIP mice). mCherry fusion tag was visualized only in the VMH of RIP-Cre mice, confirming successful expression of the transgene muscarinic receptor (Fig 8A). Treatment with CNO evoked an increase in c-Fos immunoreactivity in VMH of $hM3D_{Gq}$RIP mice (Fig 8B). $hM3D_{Gq}$RIP mice treated with CNO displayed higher energy expenditure under room temperature and were resistant to acute cold challenge when compared to those treated with vehicle (Fig 8C and D). Treatment with CNO promoted beiging of sWAT, and increased sympathetic outflow to sWAT and neuronal activity in RPa in $hM3D_{Gq}$RIP mice (Fig 8E–I), whereas BAT functions, food intake, RER, and locomotor activity were similar between the mice treated with CNO or vehicle (Fig 8E–H and Appendix Fig S6A–C). In addition, mice with activation of RIP-Cre neurons displayed normal responses to starvation (Appendix Fig S6D–F). To further support the notion that activation of VMH RIP-Cre neurons promotes beiging of sWAT via SNS, we treated the mice with the β3-adrenergic receptor antagonist SR59230A. Treatment with SR59230A abolished CNO-induced adaptive thermogenesis and beiging of sWAT but had no effect on neuronal activation in VMH and RPa of $hM3D_{Gq}$RIP mice (Fig EV5A–F). Taken together, these findings suggest that RIP-Cre neurons in VMH selectively regulate sympathetic outflow to sWAT through the β3-adrenergic receptor in response to cold challenge.

Discussion

Several regions of the hypothalamus and subsets of hypothalamic neurons have been shown to control thermogenic program in BAT and sWAT [11]. However, whether activation of brown and beige adipocytes can be differentially controlled by neuronal circuits and population remains poorly understood. The present study demonstrates that RIP-Cre neurons in VMH act as critical regulators of systemic energy balance by mediating the crosstalk between hypothalamus and sWAT via SNS. We propose a model whereby disruption of proper function of RIP-Cre neurons in VMH through APPL2 deletion leads to increased VMH AMPK activity, reduced neuronal activation in RPa, diminished sympathetic outflow to sWAT, defective beiging in sWAT, and increased adiposity (synopsis image). In contrast, activation of RIP-Cre neurons in VMH by pharmacogenetic approach exerts opposite effects. In addition, defects in cold-induced beiging by APPL2 deletion can be rescued by activation of RIP-Cre neurons or AMPK inhibition, suggesting that the regulation of APPL2 on AMPK activity is essential for proper function of RIP-Cre neurons under cold environment.

Sympathetic nervous system outflow to WAT and BAT are differentially regulated in response to different extrinsic factors such as fasting and cold exposure [12]. The differential lipolytic and thermogenic responses may be ascribed to different densities of sympathetic innervation and/or distinct hypothalamic networks to BAT and WAT [39–41]. Transneuronal viral tract tracing studies revealed that hypothalamic origins of the SNS outflow to BAT and sWAT are largely disparate, despite that some of the neuronal population (~10–20%) are overlapped [11,13,40,41]. A recent study indicated that fasting and activation of AgRP neurons in ARC control beiging selectively in sWAT without affecting BAT [16]. In this study, we demonstrated that RIP-Cre neurons in VMH regulate beiging and lipolysis preferentially in WAT but not in BAT in response to cold exposure. We showed that this neuronal population is crucial for cold-induced rather than fasting-mediated thermogenic and lipolytic responses in WAT. These findings also suggest that beiging in WAT, which can be controlled by discrete hypothalamic neurons and networks such as AgRP and RIP-Cre neurons, is a dynamic physiological protection against extreme conditions such as fasting and cold exposure, respectively.

Insulin II mRNA has been shown to be expressed in the brain of adult rat [42]. In the lower organism such as *Drosophila*, insulin-producing neurosecretory cells can sense the changes in temperature and nutrient availability, which in turn control growth and body size via secretion of insulin-like peptides [43,44]. In rodents, RIP-Cre neurons are crucial for energy balance [45–50]. This insulin II promoter-expressing neuronal population is widely distributed in many hypothalamic nuclei including ARC, VMH, and PVN, but does not overlap any known neuronal populations in the hypothalamus, yet its presence in human remains to be identified [27,46]. Disruption of leptin and insulin signaling in RIP-Cre neurons causes obesity via an unidentified mechanism [45–48]. A recent study shows that GABA released from RIP-Cre neurons in the arcuate nucleus (ARC) increases energy expenditure by promoting BAT thermogenesis [38]. In contrast, we demonstrated that RIP-Cre neurons in VMH have no effect on BAT metabolism but control SNS-dependent beiging of sWAT. Moreover, activation of mTOR in RIP-Cre neurons alters expression of the neuropeptides POMC and NPY in the hypothalamus, leading to hyperphagia and obesity [49]. These data collectively suggest that different subsets of RIP-Cre neurons play distinct roles in the regulation of energy metabolism in a fat depot-specific manner. The unique feature of RIP-Cre neurons in VMH is crucial because it selectively controls SNS outflow and beiging of sWAT but not in other tissues and has no impact on food intake. Since obese patients have increased amount of WAT but reduced amount and activity of BAT, the selective conversion of WAT to beige fat may help to combat against obesity. On the other hand, it is of importance to identify whether such neuronal population responsible for selective beiging of WAT is conserved in humans.

The differential roles of RIP-Cre neurons in ARC and VMH on energy balance may be due to their distinct neuronal connections within hypothalamus and to other brain areas and/or neurotransmitter circuits. First, RIP-Cre neurons in ARC are heterogeneous and GABAergic (i.e., release the inhibitory neurotransmitter GABA) in nature [38,51], whereas the majority of VMH neurons are glutamatergic (i.e., release the excitatory neurotransmitter glutamine) [52]. Second, RIP-Cre neurons in ARC project to the PVH, while VMH is anatomically connected to different areas of brain stem such

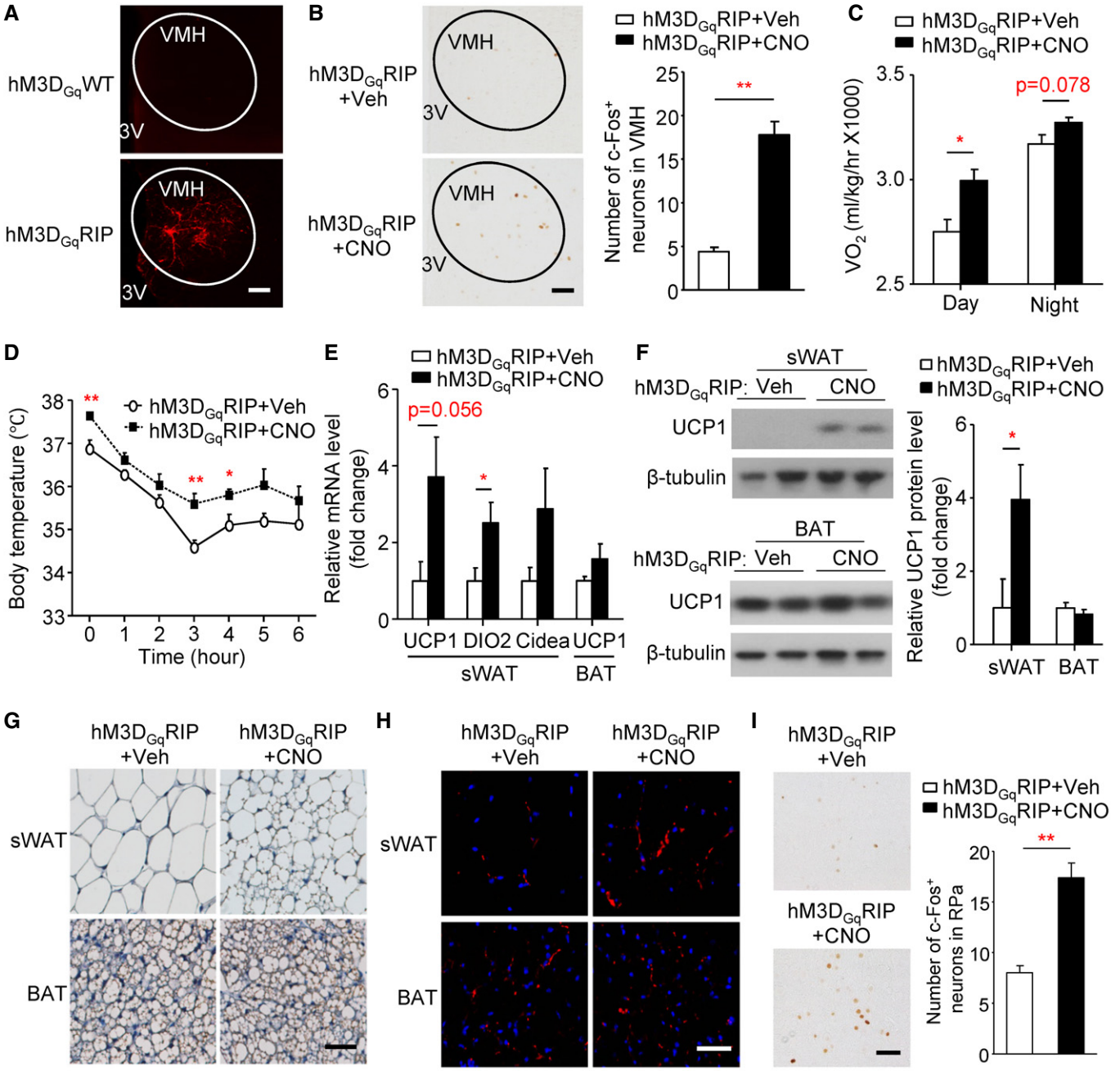

Figure 8. Activation of RIP-Cre neurons induces beiging and adaptive thermogenesis in mice.

Six-week-old male RIP-Cre mice were bilaterally injected with 2 × 10^9 viral particles of AAV-hM3Dq-mCherry into VMH to generate hM3D$_{Gq}$RIP mice. 3 weeks after injection, mice were intraperitoneally injected with CNO (0.3 mg/kg) or saline (as vehicle) every day for 21 days under 22°C. The first day of CNO injected is defined as day 1.

A mCherry fluorescent signal (red) was directly detected under a fluorescent microscope. Representative images were shown. Noted that WT mice were injected with AAV-hM3Dq-mCherry as negative control in the upper panel.

B Representative images of IHC staining of c-Fos in VMH. The right panel represents the quantification of the number of c-Fos-positive neurons in the VMH.

C Oxygen consumption of mice under 22°C (day 11).

D Mice were subjected to acute cold exposure (4°C) for 6 h at day 15. Core body temperature was measured.

E–I The mice were acclimated at 22°C for 6 days after the acute cold exposure, followed by tissues collection at day 21. (E) mRNA levels of UCP1, DIO2, and Cidea normalized with 18S in sWAT and BAT. (F) Immunoblotting analysis of UCP1 and β-tubulin in sWAT (upper panel) and BAT (lower panel). The right panel is the densitometric analysis relative abundance of UCP1 normalized with β-tubulin. (G) Representative images of IHC staining of UCP1 in sections of sWAT and BAT. (H) Representative images of IHC staining of TH (red) and DAPI (blue) in sections of sWAT and BAT. (I) Representative images of IHC staining of c-Fos in RPa. The right panel represents the quantification of the number of c-Fos-positive neurons in the RPa.

Data information: $n = 5$. Data are represented as mean ± SEM. *$P < 0.05$, **$P < 0.01$ (two-tailed independent Student's t-test). Scale bar: 50 μm.
Source data are available online for this figure.

as RPa and inferior olive [38,53,54]. Third, ARC contains heterogeneous neuronal population including POMC-, NPY-, AgRP-expressing neurons [55], whereas VMH mainly contains SF1- and Nkx2.1-expressing neurons [56]. These differences may contribute to the distinct actions of VMH and ARC RIP-Cre neurons on energy metabolism. On the other hand, it is currently unknown whether and how RIP-Cre neurons in VMH directly control SNS outflow to sWAT via RPa or indirectly via intrahypothalamic connections or neurotransmitters. Further investigations mapping the neuronal network linking VMH RIP-Cre neurons, SNS and WAT, and characterization of VMH RIP-Cre neurons (such as their molecular signature, glutamatergic, or GABAergic) are warranted.

Ventromedial hypothalamus was the first hypothalamic site identified to regulate adaptive thermogenesis [57]. Ventromedial hypothalamus lesions diminish sympathetic drives to WAT and BAT, leading to defective cold-induced lipolysis and obesity in rodents [58–60]. Various thermogenic factors, including thyroid hormone, estrogen, bone morphogenetic protein 8B (BMP8B), and glucagon-like peptide-1 (GLP-1) receptor agonist liraglutide, act on VMH to induce beiging and activation of BAT via the inhibition of AMPK pathway [5,36,61,62]. In this study, we showed that deletion of APPL2 leads to activation of AMPK in the hypothalamus, which in turn diminishes SNS outflow to sWAT and subsequent adaptive thermogenesis. As an interacting partner of the adiponectin receptors, APPL2 suppresses adiponectin-induced activation of AMPK in myotubes [22]. Indeed, we found that APPL2 interacts with AMPK in hypothalamus, and this interaction is augmented by cold exposure (Wang B. Unpublished observation). However, further study deciphering the underlying mechanism by which APPL2 regulates AMPK activity, and whether the APPL2–AMPK signaling axis is essential for the thermogenic factors (such as BMP8P and thyroid) in VMH as well as how APPL2 regulates activation of RIP-Cre neurons are warranted.

In summary, we have employed both genetic models and pharmacogenetic approaches to demonstrate that a subset of RIP-Cre neurons is crucial for activation of SNS outflow to sWAT, adaptive thermogenesis, and energy homeostasis. APPL2 deficiency in RIP-Cre neurons in VMH is an important contributor for defective beiging of sWAT, and targeted activation of RIP-Cre neurons in VMH is able to convert energy storing white adipocytes to energy burning beige adipocytes.

Materials and Methods

Animal study

All animals were sex- and age-matched, and littermates were used, as indicated in the figure legends. Animals were allocated to their experimental group according to their genotypes, and therefore, no randomization is used, unless otherwise noted. The investigators were not blinded to the experimental groups. Homozygous APPL2 floxed ($APPL2^{floxed/floxed}$) mice, generated in our previous study [21], were crossed with RIP-Cre mice ($RIP\text{-}Cre^{+}$, from Jackson Laboratory) to generate heterozygous RIP-APPL2-KO mice ($RIP\text{-}Cre^{+}$ $APPL2^{floxed/-}$) and $APPL2^{floxed/-}$ mice. $RIP\text{-}Cre^{+}APPL2^{floxed/-}$ mice were intercrossed with $APPL2^{floxed/-}$ mice to generate RIP-Cre control mice ($RIP\text{-}Cre^{+}\text{-}APPL2^{-/-}$), wild-type (WT) littermates ($APPL2^{floxed/floxed}$), and RIP-APPL2-KO mice ($RIP\text{-}Cre^{+}\text{-}APPL2^{floxed/floxed}$). RIP-Cre-GFP mice were generated by crossing Z/EG mice (with the permission of Dr. Corrinne Lobe from Sunnybrook and Women's Health Science Center in Canada, and obtained from the Transgenic Core Facility in The University of Hong Kong) with RIP-Cre mice. Genotyping of mice carrying RIP-Cre, Z/EG, and the floxed APPL2 allele was performed as previously described [21,30,63]. To generate VMH-RIP-APPL2-KO mice, 6-week-old $APPL2^{floxed/floxed}$ mice were randomly assigned to bilateral stereotaxic injection of AAV-RIP-Cre or AAV-RIP-GFP (2×10^9 viral particles) into VMH. To activate RIP-Cre neurons in RIP-APPL2-KO mice, AAV-hM3Dq-mCherry (2×10^9 viral particles) was injected into the VMH of 10-week-old RIP-APPL2-KO mice and their WT littermates. In Figs 8 and EV5, 6-week-old RIP-Cre mice injected with AAV-hM3Dq-mCherry were randomly assigned to intraperitoneal injection of CNO, SR59230A, or vehicle for 21 days. To inhibit AMPK activity (Fig 7), AAV-DN-AMPK or AAV-GFP (2×10^9 viral particles) was bilaterally injected into the VMH of 12-week-old WT and RIP-APPL2-KO mice. The above mice were maintained onto a C57BL/6 genetic background. Age-matched male RIP-APPL2-KO mice and their WT littermates and RIP-Cre controls were used in all the experiments of this study. Animals were allocated to their experimental group according to their genotypes. The mice were kept at room temperature (22°C ± 1°C) on a 12 h/12 h light/dark cycle, with *ad libitum* access to water and either fed on a STC or 45% HFD (Cat No. D12451, Research Diets). For cold challenge experiments, mice were housed at 4°C for different durations as specified in figure legends. For thermoneutral condition (30°C), the mice were housed in a small animal intensive care unit (Harvard Apparatus). Body weight and accumulative food intake were monitored on a biweekly basis. Body composition was determined using a minispec body composition analyzer (Bruker Minispec LF90). Environment-controlled comprehensive laboratory animal monitoring system (CLAMS, Columbus Instruments) was used to continuously record food intake, oxygen consumption, locomotor activity, and RER at different temperatures as indicated in the figure legends. The mice were acclimated to the system for 2–3 days before the measurement. Core body temperature during cold challenge test was measured by a thermometer with a rectal probe (Model 4610 Precision Thermometer, Measurement Specialties). All experimental protocols were approved by the Committee on the Use of Live Animals in Teaching and Research at The University of Hong Kong.

Quantitative real-time PCR (qPCR)

RNA was extracted from the tissues using TRIzol reagent (Life Technology), followed by reverse transcription using an ImProm-II reverse transcription kit (Promega) with random hexamer primers. cDNAs were processed for real-time PCR using SYBR Green master mix (Qiagen) with specific primers (Table 1) on a StepOnePlus Real-Time PCR System (Applied Biosystems). All data were normalized with *18S*.

Immunoblotting

Proteins were extracted from different fat pads and hypothalami using a RIPA lysis buffer containing 0.5% NP-40, 0.1% sodium deoxycholate, 150 mM NaCl, 50 mM Tris–HCl (pH 7.4), phosphatase inhibitors, and protease inhibitor cocktail (Roche). Equal amounts of proteins were separated by SDS–PAGE, transferred to

Table 1. Sequences of qPCR primers.

Gene names	Primer sequences	
UCP1	Forward	5′-TGG AGG TGT GGC AGT GTT CA-3′
	Reverse	5′-GCT CTG GGC TTG CAT TCT G-3′
DIO2	Forward	5′-CAG TGT GGT GCA CGT CTC CAA TC-3′
	Reverse	5′-TGA ACC AAA GTT GAC CAC CAG-3′
Cidea	Forward	5′-TGC TCT TCT GTA TCG CCC AGT-3′
	Reverse	5′-GCC GTG TTA AGG AAT CTG CTG-3′
18S	Forward	5′-GTA ACC CGT TGA ACC CCA TT-3′
	Reverse	5′-CCA TCC AAT CGG TAG TAG CG-3′
GFP (for AAV titration)	Forward	5′-GCA CAA GCT GGA GTA CAA CTA-3′
	Reverse	5′-TGT TGT GGC GGA TCT TGA A-3′
Cre (for AAV titration)	Forward	5′-CTG ACG GTG GGA GAA TGT TAA T-3′
	Reverse	5′-CAT CGC TCG ACC AGT TTA GTT-3′
mCherry (for AAV titration)	Forward	5′-ATG AAC TGA GGG GAC AGG ATG-3′
	Reverse	5′-TGG CCA TCA TCA AGG AGT TCA-3′

PVDF membranes, and probed with different primary antibodies as specified in each figure legend. Rabbit polyclonal antibodies against phospho-HSL (Ser-660; 1:1,000, Cat No. 4126), total HSL (1:1,000, Cat No. 4107), GAPDH (1:2,500, Cat No. 5174), β-tubulin (1:2,500, Cat No. 2128), phospho-AMPK (Thr-172; 1:1,000, Cat No. 2531), total AMPK (1:1,000, Cat No. 2532), phospho-ACC (Ser-79; 1:1,000, Cat No. 3661), total ACC (1:1,000, Cat No. 3662), phospho-Akt (Ser-473; 1:1,000, Cat No. 9271), total Akt (1:1,000, Cat No. 9272), and HSP90 (1:1,000, Cat No. 4874S) were from Cell Signaling Technology. Rabbit polyclonal antibody against UCP1 (1:2,500, Cat No. Ab10983) was purchased from Abcam. Rabbit polyclonal antibody against TH (1:1,000, Cat No. AB152) was from EMD Millipore. Rabbit polyclonal antibody against APPL1 (1:2,000, Cat. No. 11430) and APPL2 (1:2,000, Cat. No. 11140) was obtained from Antibody and Immunoassay Services (AIS), The University of Hong Kong (HKU). The specific signals were visualized by horseradish peroxidase-conjugated secondary antibodies (Cell Signaling Technology) and enhanced chemiluminescence reagents (GE Healthcare). Intensities of the protein bands were quantified by ImageJ software.

Histological and immunohistochemical analyses

Mice were anesthetized with an overdose of pentobarbital (200 mg/kg) for intracardial perfusion of PBS, followed by 4% paraformaldehyde (PFA) in phosphate buffer (0.1 M, pH 7.4). Brains, pancreases, and different fat depots were post-fixed overnight in 4% PFA, dehydrated and embedded with paraffin, and then sectioned at the thickness of 5 μm. The paraffin sections of adipose tissues were stained with hematoxylin and eosin. For immunofluorescence staining, deparaffinized and rehydrated sections were subjected to antigen retrieval in a sodium citrate buffer (10 mM sodium citrate, 0.05% Tween-20, pH 6.0) at 99°C for 20 min. Sections were blocked with 10% fetal bovine serum (FBS) and 3% bovine serum albumin (BSA) in PBS for 1 h at room temperature and incubated with anti-APPL2 (1:200, mouse polyclonal, Abnova #H00055198-B01P or 1:200, rabbit polyclonal, AIS, HKU), anti-insulin (1:500, mouse monoclonal, HyTest #2IP10-D6C4), anti-GFP (1:100, rabbit polyclonal, Santa Cruz #sc-8334 or 1:200, mouse monoclonal, Abcam #ab1218), anti-Cre (1:200, rabbit polyclonal, Millipore #69050), anti-Nkx2.1 (1:200, rabbit monoclonal, Abcam #ab76013), anti-c-Fos (1:200, mouse monoclonal, Abcam #ab208942), or anti-TH (1:500, rabbit polyclonal, Millipore #AB152) antibody in 3% BSA overnight at 4°C. After washing three times with PBS, the sections were incubated with secondary antibodies (Alexa Fluor 488 anti-Rabbit IgG, Alexa Fluor 594 anti-Rabbit IgG, Alexa Fluor 488 anti-Mouse IgG, or Alexa Fluor 594 anti-Mouse IgG, 1:500, Thermo Fisher Scientific) for 1 h at room temperature. Nuclei were counterstained by 4′, 6-diamidino-2-phenylindole (DAPI, 10 ng/ml, Thermo Fisher Scientific #P36931). For immunohistochemistry, tissue slides were incubated with anti-UCP1 (1:500, rabbit polyclonal, Abcam #ab10983) or anti-c-Fos (1:200, mouse monoclonal, Abcam #ab208942) antibody overnight at 4°C, followed by incubation with horseradish peroxidase-conjugated secondary antibodies against rabbit IgG (Cell Signaling Technology), and developed by SIGMAFAST 3, 3′ diaminobenzidine (DAB) tablets (Sigma-Aldrich) with counterstaining for nuclei using hematoxylin solution. All the slides were visualized with an Olympus biological microscope BX41. Images were captured using an Olympus DP72 color digital camera. The intensities of positively stained cells were quantified in each of five randomly selected fields by the ImageJ software. Two independent investigators blinded to sample identity: one investigator performed the staining and another investigator analyzed the tissue sections.

Measurement of norepinephrine content in peripheral tissues

To determine the norepinephrine contents in tissues, mice were anesthetized with pentobarbital (200 mg/kg). Adipose tissues, livers, and kidneys were immediately dissected and homogenized in 0.01 N HCl in the presence of EDTA (1 mM) and sodium metabisulfite (4 mM). Norepinephrine was extracted from 550 μl tissue lysates using a cis-diol-specific affinity gel, acylated, derivatized enzymatically, and then measured with a competitive ELISA kit (Abnova #KA3836).

Generation of adeno-associated virus (AAV)

To construct pAAV-RIP-GFP, RIP coding sequence was amplified from pRIP-Cre-GH (Labnodes) by PCR. The PCR product and pAAV-CMV-GFP vector (Vector Biolabs) were digested with MluI and BamHI at 37°C for overnight and were then ligated by T4 DNA ligase (NEB) to generate pAAV-RIP-GFP. To construct pAAV-RIP-Cre, RIP-Cre sequence was amplified from pRIP-Cre-GH by PCR. This PCR product containing the RIP-Cre sequence, together with pAAV-mIP2-GFP vector [63], was digested with MluI and XhoI for overnight at 37°C, and was subsequently ligated to generate pAAV-RIP-Cre. The AAV-hSyn-DIO-hM3D(Gq)-mCherry (AAV-hM3Dq-mCherry) plasmid was obtained from Addgene (#44361). A dominant-negative form AMPK-alpha-2 (D159A) was cloned into AAV-CMV vector, which is so-called AAV-AMPK-DN [64]. The AAV vector plasmid was cotransfected with pAAV2 rep cap, and pAAV helper plasmids into HEK293 cells were obtained from American Type Culture Collection and free of mycoplasma contamination.

AAVs (serotype 2) were purified by polyethylene glycol/aqueous two-phase partitioning method and were titrated by qPCR analysis as we previously described [25,63].

Stereotaxic injection of AAV

Mice were anesthetized with ketamine (400 mg/kg) and xylazine (40 mg/kg) and placed in a stereotaxic apparatus (Harvard Apparatus). AAV-RIP-GFP, AAV-RIP-Cre, AAV-GFP, AAV-DN-AMPK or AAV-hM3Dq-mCherry (2×10^9 viral particles) were bilaterally injected into VMH (coordinates, bregma: anterior–posterior, −1.4 mm; dorsal–ventral, −5.6 mm; lateral, ±0.4 mm, 2 μl/side) of the mice using a 5-μl Hamilton syringe, followed by recovery and AAV expression for 3 weeks. For those administered with AAV-hM3Dq-mCherry, mice received daily intraperitoneal injections of CNO (0.3 mg/kg, Sigma-Aldrich) or saline (as vehicle) for 6 days at room temperature, followed by consecutive daily injections for 10 days in the cold environment.

Statistical analysis

All statistical analyses were performed using Prism 6 (GraphPad Software Inc.) or SPSS. Animal sample size for each study was chosen on the basis of literature documentation of similar well-characterized experiments, and no statistical method was used to predetermine sample size. Data were presented as mean ± SEM. Statistical significance was assessed by two-tailed independent Student's *t*-test or one-way ANOVA with Bonferroni correction for multiple comparisons. A value of $P < 0.05$ was considered statistically significant.

Data availability

The data supporting the findings of this study are available within the article and its Supplementary Information Files or are available from the corresponding author upon reasonable request.

Expanded View for this article is available online.

Acknowledgements
This work was supported by Health Medical Research Fund 02131606, National 973 Basic Research Program of China (2015CB553603), National Natural Science Foundation of China (81270881), General Research Fund (17101815), and HKU matching fund for The State Key laboratory of Pharmaceutical Biotechnology. We thank Dr. Andras Nagy (Lunenfeld-Tanenbaum Research Institute) for providing Z/EG mice.

Author contributions
BW designed and carried out the experiments, analyzed and interpreted the results, and wrote the manuscript. AL interpreted the results and reviewed the manuscript. XL and PWLH conducted the experiments. DW performed experiments and wrote manuscript. XW, ZL, and KKLW contributed to study experimental results. AX and SSYY designed the study and reviewed the manuscript. KKYC designed the study, analyzed and interpreted the results, and wrote and edited the manuscript.

Conflict of interest
The authors declare that they have no conflict of interest.

References

1. Kajimura S, Spiegelman BM, Seale P (2015) Brown and beige fat: physiological roles beyond heat generation. *Cell Metab* 22: 546 – 559
2. Schulz TJ, Tseng Y-H (2013) Brown adipose tissue: development, metabolism and beyond. *Biochem J* 453: 167 – 178
3. van Marken Lichtenbelt WD, Vanhommerig JW, Smulders NM, Drossaerts JM, Kemerink GJ, Bouvy ND, Schrauwen P, Teule GJ (2009) Cold-activated brown adipose tissue in healthy men. *N Engl J Med* 360: 1500 – 1508
4. Yoneshiro T, Aita S, Matsushita M, Okamatsu-Ogura Y, Kameya T, Kawai Y, Miyagawa M, Tsujisaki M, Saito M (2011) Age-related decrease in cold-activated brown adipose tissue and accumulation of body fat in healthy humans. *Obesity* 19: 1755 – 1760
5. Whittle AJ, Carobbio S, Martins L, Slawik M, Hondares E, Vazquez MJ, Morgan D, Csikasz RI, Gallego R, Rodriguez-Cuenca S *et al* (2012) BMP8B increases brown adipose tissue thermogenesis through both central and peripheral actions. *Cell* 149: 871 – 885
6. Bostrom P, Wu J, Jedrychowski MP, Korde A, Ye L, Lo JC, Rasbach KA, Bostrom EA, Choi JH, Long JZ *et al* (2012) A PGC1-alpha-dependent myokine that drives brown-fat-like development of white fat and thermogenesis. *Nature* 481: 463 – 468
7. Fisher FM, Kleiner S, Douris N, Fox EC, Mepani RJ, Verdeguer F, Wu J, Kharitonenkov A, Flier JS, Maratos-Flier E *et al* (2012) FGF21 regulates PGC-1alpha and browning of white adipose tissues in adaptive thermogenesis. *Genes Dev* 26: 271 – 281
8. Bartelt A, Bruns OT, Reimer R, Hohenberg H, Ittrich H, Peldschus K, Kaul MG, Tromsdorf UI, Weller H, Waurisch C (2011) Brown adipose tissue activity controls triglyceride clearance. *Nat Med* 17: 200 – 205
9. Berbée JF, Boon MR, Khedoe PPS, Bartelt A, Schlein C, Worthmann A, Kooijman S, Hoeke G, Mol IM, John C (2015) Brown fat activation reduces hypercholesterolaemia and protects from atherosclerosis development. *Nat Commun* 6: 6356
10. Bartelt A, Heeren J (2014) Adipose tissue browning and metabolic health. *Nat Rev Endocrinol* 10: 24 – 36
11. Stefanidis A, Wiedmann N, Adler E, Oldfield B (2014) Hypothalamic control of adipose tissue. *Best Pract Res Clin Endocrinol Metab* 28: 685 – 701
12. Brito NA, Brito MN, Bartness TJ (2008) Differential sympathetic drive to adipose tissues after food deprivation, cold exposure or glucoprivation. *Am J Physiol Regul Integr Comp Physiol* 294: R1445 – R1452
13. Nguyen NLT, Barr CL, Ryu V, Cao Q, Xue B, Bartness TJ (2017) Separate and shared sympathetic outflow to white and brown fat coordinately regulates thermoregulation and beige adipocyte recruitment. *Am J Physiol Regul Integr Comp Physiol* 312: R132 – R145
14. Fischer K, Ruiz HH, Jhun K, Finan B, Oberlin DJ, van der Heide V, Kalinovich AV, Petrovic N, Wolf Y, Clemmensen C *et al* (2017) Alternatively activated macrophages do not synthesize catecholamines or contribute to adipose tissue adaptive thermogenesis. *Nat Med* 23: 623 – 630
15. Townsend K, Tseng Y-H (2012) Brown adipose tissue: recent insights into development, metabolic function and therapeutic potential. *Adipocyte* 1: 13 – 24
16. Ruan HB, Dietrich MO, Liu ZW, Zimmer MR, Li MD, Singh JP, Zhang K, Yin R, Wu J, Horvath TL *et al* (2014) O-GlcNAc transferase enables AgRP neurons to suppress browning of white fat. *Cell* 159: 306 – 317
17. Dodd GT, Decherf S, Loh K, Simonds SE, Wiede F, Balland E, Merry TL, Munzberg H, Zhang ZY, Kahn BB *et al* (2015) Leptin and insulin act on POMC neurons to promote the browning of white fat. *Cell* 160: 88 – 104

18. Orozco-Solis R, Aguilar-Arnal L, Murakami M, Peruquetti R, Ramadori G, Coppari R, Sassone-Corsi P (2016) The circadian clock in the ventromedial hypothalamus controls cyclic energy expenditure. *Cell Metab* 23: 467 – 478
19. Miaczynska M, Christoforidis S, Giner A, Shevchenko A, Uttenweiler-Joseph S, Habermann B, Wilm M, Parton RG, Zerial M (2004) APPL proteins link Rab5 to nuclear signal transduction via an endosomal compartment. *Cell* 116: 445 – 456
20. Cheng KK, Lam KS, Wang B, Xu A (2014) Signaling mechanisms underlying the insulin-sensitizing effects of adiponectin. *Best Pract Res Clin Endocrinol Metab* 28: 3 – 13
21. Cheng KK, Zhu W, Chen B, Wang Y, Wu D, Sweeney G, Wang B, Lam KS, Xu A (2014) The adaptor protein APPL2 inhibits insulin-stimulated glucose uptake by interacting with TBC1D1 in skeletal muscle. *Diabetes* 63: 3748 – 3758
22. Wang C, Xin X, Xiang R, Ramos FJ, Liu M, Lee HJ, Chen H, Mao X, Kikani CK, Liu F *et al* (2009) Yin-Yang regulation of adiponectin signaling by APPL isoforms in muscle cells. *J Biol Chem* 284: 31608 – 31615
23. Cleasby ME, Lau Q, Polkinghorne E, Patel SA, Leslie SJ, Turner N, Cooney G, Xu A, Kraegen E (2011) The adaptor protein APPL1 increases glycogen accumulation in rat skeletal muscle through activation of the PI3-kinase signalling pathway. *J Endocrinol* 210: 81 – 92
24. Cheng KK, Lam KS, Wu D, Wang Y, Sweeney G, Hoo RL, Zhang J, Xu A (2012) APPL1 potentiates insulin secretion in pancreatic beta cells by enhancing protein kinase Akt-dependent expression of SNARE proteins in mice. *Proc Natl Acad Sci USA* 109: 8919 – 8924
25. Jiang X, Zhou Y, Wu KK, Chen Z, Xu A, Cheng KK (2017) APPL1 prevents pancreatic beta cell death and inflammation by dampening NFkappaB activation in a mouse model of type 1 diabetes. *Diabetologia* 60: 464 – 474
26. Prudente S, Jungtrakoon P, Marucci A, Ludovico O, Buranasupkajorn P, Mazza T, Hastings T, Milano T, Morini E, Mercuri L *et al* (2015) Loss-of-function mutations in APPL1 in familial diabetes mellitus. *Am J Hum Genet* 97: 177 – 185
27. Wicksteed B, Brissova M, Yan W, Opland DM, Plank JL, Reinert RB, Dickson LM, Tamarina NA, Philipson LH, Shostak A *et al* (2010) Conditional gene targeting in mouse pancreatic ss-Cells: analysis of ectopic Cre transgene expression in the brain. *Diabetes* 59: 3090 – 3098
28. Davis AM, Seney ML, Stallings NR, Zhao L, Parker KL, Tobet SA (2004) Loss of steroidogenic factor 1 alters cellular topography in the mouse ventromedial nucleus of the hypothalamus. *J Neurobiol* 60: 424 – 436
29. Sussel L, Marin O, Kimura S, Rubenstein JL (1999) Loss of Nkx2.1 homeobox gene function results in a ventral to dorsal molecular respecification within the basal telencephalon: evidence for a transformation of the pallidum into the striatum. *Development* 126: 3359 – 3370
30. Novak A, Guo C, Yang W, Nagy A, Lobe CG (2000) Z/EG, a double reporter mouse line that expresses enhanced green fluorescent protein upon Cre-mediated excision. *Genesis* 28: 147 – 155
31. Lowell BB, Spiegelman BM (2000) Towards a molecular understanding of adaptive thermogenesis. *Nature* 404: 652 – 660
32. Cannon B, Nedergaard J (2004) Brown adipose tissue: function and physiological significance. *Physiol Rev* 84: 277 – 359
33. Jakus PB, Sandor A, Janaky T, Farkas V (2008) Cooperation between BAT and WAT of rats in thermogenesis in response to cold, and the mechanism of glycogen accumulation in BAT during reacclimation. *J Lipid Res* 49: 332 – 339
34. Morrison SF, Nakamura K (2011) Central neural pathways for thermoregulation. *Front Biosci* 16: 74
35. Ray RS, Corcoran AE, Brust RD, Kim JC, Richerson GB, Nattie E, Dymecki SM (2011) Impaired respiratory and body temperature control upon acute serotonergic neuron inhibition. *Science* 333: 637 – 642
36. López M, Varela L, Vázquez MJ, Rodríguez-Cuenca S, González CR, Velagapudi VR, Morgan DA, Schoenmakers E, Agassandian K, Lage R (2010) Hypothalamic AMPK and fatty acid metabolism mediate thyroid regulation of energy balance. *Nat Med* 16: 1001 – 1008
37. Lopez M, Nogueiras R, Tena-Sempere M, Dieguez C (2016) Hypothalamic AMPK: a canonical regulator of whole-body energy balance. *Nat Rev Endocrinol* 12: 421 – 432
38. Kong D, Tong Q, Ye C, Koda S, Fuller PM, Krashes MJ, Vong L, Ray RS, Olson DP, Lowell BB (2012) GABAergic RIP-Cre neurons in the arcuate nucleus selectively regulate energy expenditure. *Cell* 151: 645 – 657
39. Murano I, Barbatelli G, Giordano A, Cinti S (2009) Noradrenergic parenchymal nerve fiber branching after cold acclimatisation correlates with brown adipocyte density in mouse adipose organ. *J Anat* 214: 171 – 178
40. Bamshad M, Song CK, Bartness TJ (1999) CNS origins of the sympathetic nervous system outflow to brown adipose tissue. *Am J Physiol* 276: R1569 – R1578
41. Bamshad M, Aoki VT, Adkison MG, Warren WS, Bartness TJ (1998) Central nervous system origins of the sympathetic nervous system outflow to white adipose tissue. *Am J Physiol* 275: R291 – R299
42. Devaskar SU, Singh BS, Carnaghi LR, Rajakumar PA, Giddings SJ (1993) Insulin II gene expression in rat central nervous system. *Regul Pept* 48: 55 – 63
43. Li Q, Gong Z (2015) Cold-sensing regulates *Drosophila* growth through insulin-producing cells. *Nat Commun* 6: 10083
44. Ikeya T, Galic M, Belawat P, Nairz K, Hafen E (2002) Nutrient-dependent expression of insulin-like peptides from neuroendocrine cells in the CNS contributes to growth regulation in *Drosophila*. *Curr Biol* 12: 1293 – 1300
45. Covey SD, Wideman RD, McDonald C, Unniappan S, Huynh F, Asadi A, Speck M, Webber T, Chua SC, Kieffer TJ (2006) The pancreatic beta cell is a key site for mediating the effects of leptin on glucose homeostasis. *Cell Metab* 4: 291 – 302
46. Choudhury AI, Heffron H, Smith MA, Al-Qassab H, Xu AW, Selman C, Simmgen M, Clements M, Claret M, Maccoll G *et al* (2005) The role of insulin receptor substrate 2 in hypothalamic and beta cell function. *J Clin Invest* 115: 940 – 950
47. Kubota N, Terauchi Y, Tobe K, Yano W, Suzuki R, Ueki K, Takamoto I, Satoh H, Maki T, Kubota T *et al* (2004) Insulin receptor substrate 2 plays a crucial role in beta cells and the hypothalamus. *J Clin Invest* 114: 917 – 927
48. Lin X, Taguchi A, Park S, Kushner JA, Li F, Li Y, White MF (2004) Dysregulation of insulin receptor substrate 2 in beta cells and brain causes obesity and diabetes. *J Clin Invest* 114: 908 – 916
49. Mori H, Inoki K, Munzberg H, Opland D, Faouzi M, Villanueva EC, Ikenoue T, Kwiatkowski D, MacDougald OA, Myers MG Jr *et al* (2009) Critical role for hypothalamic mTOR activity in energy balance. *Cell Metab* 9: 362 – 374
50. Cui Y, Huang L, Elefteriou F, Yang G, Shelton JM, Giles JE, Oz OK, Pourbahrami T, Lu CY, Richardson JA (2004) Essential role of STAT3 in body weight and glucose homeostasis. *Mol Cell Biol* 24: 258 – 269
51. Campbell JN, Macosko EZ, Fenselau H, Pers TH, Lyubetskaya A, Tenen D, Goldman M, Verstegen AM, Resch JM, McCarroll SA *et al* (2017) A molecular census of arcuate hypothalamus and median eminence cell types. *Nat Neurosci* 20: 484 – 496

52. Tong Q, Ye C, McCrimmon RJ, Dhillon H, Choi B, Kramer MD, Yu J, Yang Z, Christiansen LM, Lee CE *et al* (2007) Synaptic glutamate release by ventromedial hypothalamic neurons is part of the neurocircuitry that prevents hypoglycemia. *Cell Metab* 5: 383 – 393
53. Contreras C, Nogueiras R, Dieguez C, Rahmouni K, Lopez M (2017) Traveling from the hypothalamus to the adipose tissue: the thermogenic pathway. *Redox Biol* 12: 854 – 863
54. Lindberg D, Chen P, Li C (2013) Conditional viral tracing reveals that steroidogenic factor 1-positive neurons of the dorsomedial subdivision of the ventromedial hypothalamus project to autonomic centers of the hypothalamus and hindbrain. *J Comp Neurol* 521: 3167 – 3190
55. Cowley MA, Smart JL, Rubinstein M, Cerdan MG, Diano S, Horvath TL, Cone RD, Low MJ (2001) Leptin activates anorexigenic POMC neurons through a neural network in the arcuate nucleus. *Nature* 411: 480 – 484
56. Kurrasch DM, Cheung CC, Lee FY, Tran PV, Hata K, Ingraham HA (2007) The neonatal ventromedial hypothalamus transcriptome reveals novel markers with spatially distinct patterning. *J Neurosci* 27: 13624 – 13634
57. Hetherington A (1941) The relation of various hypothalamic lesions to adiposity and other phenomena in the rat. *Am J Physiol* 133: 326 – 327
58. Nishizawa Y, Bray GA (1978) Ventromedial hypothalamic lesions and the mobilization of fatty acids. *J Clin Invest* 61: 714
59. Vander Tuig J, Kerner J, Romsos DR (1985) Hypothalamic obesity, brown adipose tissue, and sympathoadrenal activity in rats. *Am J Physiol Endocrinol Metab* 248: E607 – E617
60. Elmquist JK, Elias CF, Saper CB (1999) From lesions to leptin: hypothalamic control of food intake and body weight. *Neuron* 22: 221 – 232
61. Xu Y, Nedungadi TP, Zhu L, Sobhani N, Irani BG, Davis KE, Zhang X, Zou F, Gent LM, Hahner LD *et al* (2011) Distinct hypothalamic neurons mediate estrogenic effects on energy homeostasis and reproduction. *Cell Metab* 14: 453 – 465
62. Beiroa D, Imbernon M, Gallego R, Senra A, Herranz D, Villarroya F, Serrano M, Ferno J, Salvador J, Escalada J *et al* (2014) GLP-1 agonism stimulates brown adipose tissue thermogenesis and browning through hypothalamic AMPK. *Diabetes* 63: 3346 – 3358
63. Li X, Cheng KK, Liu Z, Yang JK, Wang B, Jiang X, Zhou Y, Hallenborg P, Hoo RL, Lam KS *et al* (2016) The MDM2-p53-pyruvate carboxylase signalling axis couples mitochondrial metabolism to glucose-stimulated insulin secretion in pancreatic beta-cells. *Nat Commun* 7: 11740
64. Kim SY, Jeong S, Jung E, Baik KH, Chang MH, Kim SA, Shim JH, Chun E, Lee KY (2012) AMP-activated protein kinase-alpha1 as an activating kinase of TGF-beta-activated kinase 1 has a key role in inflammatory signals. *Cell Death Dis* 3: e357

